

Higgs compositeness in $\text{Sp}(2N)$ gauge theories – Determining the low-energy constants with lattice calculations *

Ed Bennett^{1,**,}, Deog Ki Hong^{2,***,}, Jong-Wan Lee^{2,3,***,}, C.-J. David Lin^{4,****,},
Biagio Lucini^{5,†,‡,}, Maurizio Piai^{6,‡,} and Davide Vadacchino^{1,**,‡}

¹Swansea Academy of Advanced Computing, Swansea University, Singleton Park, Swansea, SA2 8PP, UK

²Department of Physics, Pusan National University, Busan 46241, Korea

³Extreme Physics Institute, Pusan National University, Busan 46241, Korea

⁴Institute of Physics, National Chiao-Tung University, Hsinchu 30010, Taiwan

⁵Department of Mathematics, Swansea University, Singleton Park, Swansea, SA2 8PP, UK

⁶Department of Physics, Swansea University, Singleton Park, Swansea, SA2 8PP, UK

Abstract. As a first step towards a quantitative understanding of the $\text{SU}(4)/\text{Sp}(4)$ composite Higgs model through lattice calculations, we discuss the low energy effective field theory resulting from the $\text{SU}(4) \rightarrow \text{Sp}(4)$ global symmetry breaking pattern. We then consider an $\text{Sp}(4)$ gauge theory with two Dirac fermion flavours in the fundamental representation on a lattice, which provides a concrete example of the microscopic realisation of the $\text{SU}(4)/\text{Sp}(4)$ composite Higgs model. For this system, we outline a programme of numerical simulations aiming at the determination of the low-energy constants of the effective field theory and we test the method on the quenched theory. We also report early results from dynamical simulations, focussing on the phase structure of the lattice theory and a calculation of the lowest-lying meson spectrum at coarse lattice spacing.

1 Introduction

In its conventional (and currently accepted) formulation, the Standard Model includes an elementary Higgs field, whose condensate breaks the electroweak symmetry. While this theory predicts all currently measured observables to an impressive degree of accuracy, the presence of an elementary scalar raises conceptual issues, one of the main ones being the *hierarchy problem*. The latter expression refers to the fact that the mass of the Higgs boson (measured at around 125 GeV) is much smaller than the natural cut-off scale, the Planck scale (which is of the order of 10^{19} GeV). A possible explanation of this puzzle could rely on the assumption that the Higgs boson is not an elementary particle, but a

*Combined contributions of B. Lucini (e-mail: b.lucini@swansea.ac.uk) and J.-W. Lee (e-mail: wlee823@pusan.ac.kr).

**Funded by the Supercomputing Wales project, which is part-funded by the European Regional Development Fund (ERDF) via Welsh Government.

***Supported in part by Korea Research Fellowship program funded by the Ministry of Science, ICT and Future Planning through the National Research Foundation of Korea (2016H1D3A1909283) and under the framework of international cooperation program (NRF-2016K2A9A1A01952069).

****Supported by Taiwanese MoST grant 105-2628-M-009-003-MY4.

†Supported in part by the Royal Society and the Wolfson Foundation.

‡Supported in part by the STFC Consolidated Grants ST/L000369/1 and ST/P00055X/1.

bound state resulting from a novel strong interaction. The current experimental results show that no new particle is observed in a range of energies up to a few TeV. Hence, even assuming that we can solve the hierarchy problem with a non-elementary Higgs, we still need to face a question related to the naturalness of the scales involved, since the Higgs mass would anyhow be significantly lower than that of other states of the novel strong interaction. This is known as the *little hierarchy problem*.

Higgs compositeness [1], i.e. the framework in which the Higgs boson arises as a pseudo-Nambu-Goldstone boson (PNGB) of a novel strong interaction, provides an elegant way to circumvent the hierarchy problems of the Standard Model (see [2] for a recent review). In order to study this approach to compositeness, the first step is to understand the global symmetry breaking pattern in the novel strong force, which has to be compatible with the symmetries of the Standard Model. We start by considering the patterns of possible global symmetry breaking in gauge theories with gauge group \mathcal{G} and N_f flavours of Dirac fermions in the fundamental representation. In this scenario, depending on G , relevant possibilities for the symmetry breaking pattern $G \mapsto H$ are the following (see e.g. [3]):

1. $SU(N_f)_V \times SU(N_f)_A \mapsto SU(N_f)_V$ if $\mathcal{G} \equiv SU(N)$, $N > 2$;
2. $SU(2 N_f) \mapsto SO(2 N_f)$ if the gauge group \mathcal{G} is real;
3. $SU(2 N_f) \mapsto Sp(2 N_f)$ if the gauge group \mathcal{G} is pseudoreal.

In the PNGB scenario for the Higgs field, the electroweak gauge group of the Standard Model is embedded in H , leading to the chain of embeddings $SU(2)_L \times U(1)_Y \subset H \subset G$. Hence, in this framework it is a necessary condition that H be large enough to allow for embeddings of the Standard Model $SU(2)_L \times U(1)_Y$. The four components of the Standard Model Higgs fields are then identified with four of the pions resulting from the global symmetry breaking. Gauge theories whose dynamics is expected to be compatible with the PNGB Higgs scenario have been discussed analytically in [4–7].

The Lattice provides a robust framework for a non-perturbative analysis of the global symmetry breaking mechanism that suggests the possible interpretation of the Higgs as a PNGB. Lattice studies in this direction have started to appear only quite recently. Examples of recent and current numerical work on relevant models (some of which have been reviewed in [8]) include [9–14]. In this contribution we provide the first (and still preliminary) numerical study of the $Sp(4)$ gauge theory with $N_f = 2$ fundamental Dirac fermions. Since $Sp(4)$ is pseudoreal, according to our previous discussion, the expected global symmetry breaking pattern in this case is

$$SU(4) \mapsto Sp(4) . \tag{1}$$

As it will be clear from our discussion below, at this level this symmetry breaking pattern has the requested properties: there are five broken generators (hence, supporting via the Goldstone theorem the existence of five massless bosons, four of which can be identified with the Higgs doublet field) and the residual symmetry group $Sp(4)$ has rank two, which means that two independent $SU(2)$ subgroups can be embedded into it, hence allowing for the possibility of embedding an $SU(2)_L \times U(1)_Y$ group.

The rest of this work is organised as follows. In Sect. 2 we describe the elementary gauge theory. For the latter, using the framework of hidden local symmetry, an effective Lagrangian is obtained in Sect. 3. Section 4 is devoted to the formulation of the lattice theory and of the observables we shall compute. Our numerical results for the quenched setup and the resulting low-energy constants in the effective field theory (EFT) approach are discussed in Sect. 5. Some exploratory numerical calculations in the theory with dynamical fermions are reported in Sect. 6. In Sect. 7 we summarise our findings and we outline future directions of our work. Two companion contributions describe respectively the study of the spectrum of $Sp(4)$ Yang-Mills theory [15] and some more technical details (in particular, scale setting and topology) of Monte Carlo calculations in Yang-Mills $Sp(4)$ and in the theory with dynamical fermions [16].

2 The model

Before analysing the structure of the global symmetry breaking pattern in $\text{Sp}(2N)$ gauge theories with N_f fundamental Dirac fermions (of which the specific model we investigate numerically, $\text{Sp}(4)$ with two Dirac fermions, is a particular case), we review the properties of $\text{Sp}(2N)$ groups.

$\text{Sp}(2N)$ can be defined as the subgroup of $\text{SU}(2N)$ whose elements U fulfil the condition

$$U\Omega U^T = \Omega, \quad \Omega = \begin{pmatrix} 0 & \mathbb{I} \\ -\mathbb{I} & 0 \end{pmatrix}, \quad (2)$$

with \mathbb{I} the $N \times N$ identity. Ω is known as the *symplectic matrix*. The request of the invariance of Ω under the action of U constrains the structure of the latter as follows:

$$U = \begin{pmatrix} A & B \\ -B^* & A^* \end{pmatrix}, \quad \text{with } AA^\dagger + BB^\dagger = \mathbb{I} \text{ and } A^T B = B^T A, \quad (3)$$

where A and B are $N \times N$ matrices. For an element \mathbf{u} in the algebra of $\text{Sp}(2N)$, this implies

$$\mathbf{u} = \begin{pmatrix} \mathbf{a} & \mathbf{b} \\ \mathbf{b}^* & -\mathbf{a}^* \end{pmatrix}, \quad \text{with } \mathbf{a} = \mathbf{a}^\dagger \text{ and } \mathbf{b} = \mathbf{b}^T, \quad (4)$$

and again \mathbf{a} and \mathbf{b} are $N \times N$ matrices. Other properties of the $\text{Sp}(2N)$ group that are of interest to us here are:

1. The dimension of the group is $N(2N + 1)$;
2. The group is pseudoreal;
3. The group has rank N .

In particular, the third property means that $\text{Sp}(2N)$ contains N independent $\text{SU}(2)$ subgroups.

As a way of an example, and as a reference for the numerical part, a possible explicit embedding of the $\text{Sp}(4)$ generators onto $\text{SU}(4)$ is:

$$\begin{aligned} T^6 &= \frac{1}{2\sqrt{2}} \begin{pmatrix} 0 & 0 & -i & 0 \\ 0 & 0 & 0 & -i \\ i & 0 & 0 & 0 \\ 0 & i & 0 & 0 \end{pmatrix}, & T^7 &= \frac{1}{2\sqrt{2}} \begin{pmatrix} 0 & 0 & 0 & -i \\ 0 & 0 & -i & 0 \\ 0 & i & 0 & 0 \\ i & 0 & 0 & 0 \end{pmatrix}, \\ T^8 &= \frac{1}{2\sqrt{2}} \begin{pmatrix} 0 & -i & 0 & 0 \\ i & 0 & 0 & 0 \\ 0 & 0 & 0 & -i \\ 0 & 0 & i & 0 \end{pmatrix}, & T^9 &= \frac{1}{2\sqrt{2}} \begin{pmatrix} 0 & 0 & -i & 0 \\ 0 & 0 & 0 & i \\ i & 0 & 0 & 0 \\ 0 & -i & 0 & 0 \end{pmatrix}, \\ T^{10} &= \frac{1}{2} \begin{pmatrix} 0 & 0 & 1 & 0 \\ 0 & 0 & 0 & 0 \\ 1 & 0 & 0 & 0 \\ 0 & 0 & 0 & 0 \end{pmatrix}, & T^{11} &= \frac{1}{2\sqrt{2}} \begin{pmatrix} 0 & 0 & 0 & 1 \\ 0 & 0 & 1 & 0 \\ 0 & 1 & 0 & 0 \\ 1 & 0 & 0 & 0 \end{pmatrix}, \\ T^{12} &= \frac{1}{2} \begin{pmatrix} 0 & 0 & 0 & 0 \\ 0 & 0 & 0 & 1 \\ 0 & 0 & 0 & 0 \\ 0 & 1 & 0 & 0 \end{pmatrix}, & T^{13} &= \frac{1}{2\sqrt{2}} \begin{pmatrix} 0 & 1 & 0 & 0 \\ 1 & 0 & 0 & 0 \\ 0 & 0 & 0 & -1 \\ 0 & 0 & -1 & 0 \end{pmatrix}, \\ T^{14} &= \frac{1}{2\sqrt{2}} \begin{pmatrix} 1 & 0 & 0 & 0 \\ 0 & -1 & 0 & 0 \\ 0 & 0 & -1 & 0 \\ 0 & 0 & 0 & 1 \end{pmatrix}, & T^{15} &= \frac{1}{2\sqrt{2}} \begin{pmatrix} 1 & 0 & 0 & 0 \\ 0 & 1 & 0 & 0 \\ 0 & 0 & -1 & 0 \\ 0 & 0 & 0 & -1 \end{pmatrix}. \end{aligned} \quad (5)$$

Table 1. The field content of the theory. The two columns indicate the transformation laws under Sp(4) gauge and global SU(4).

Fields	Sp(4)	SU(4)
V_μ	10	1
Q	4	4
Σ_0	1	6
M	1	6

A choice for the generators in the coset is

$$\begin{aligned}
 T^1 &= \frac{1}{2\sqrt{2}} \begin{pmatrix} 0 & 1 & 0 & 0 \\ 1 & 0 & 0 & 0 \\ 0 & 0 & 0 & 1 \\ 0 & 0 & 1 & 0 \end{pmatrix}, & T^2 &= \frac{1}{2\sqrt{2}} \begin{pmatrix} 0 & -i & 0 & 0 \\ i & 0 & 0 & 0 \\ 0 & 0 & 0 & i \\ 0 & 0 & -i & 0 \end{pmatrix}, \\
 T^3 &= \frac{1}{2\sqrt{2}} \begin{pmatrix} 1 & 0 & 0 & 0 \\ 0 & -1 & 0 & 0 \\ 0 & 0 & 1 & 0 \\ 0 & 0 & 0 & -1 \end{pmatrix}, & T^4 &= \frac{1}{2\sqrt{2}} \begin{pmatrix} 0 & 0 & 0 & -i \\ 0 & 0 & i & 0 \\ 0 & -i & 0 & 0 \\ i & 0 & 0 & 0 \end{pmatrix}, \\
 T^5 &= \frac{1}{2\sqrt{2}} \begin{pmatrix} 0 & 0 & 0 & 1 \\ 0 & 0 & -1 & 0 \\ 0 & -1 & 0 & 0 \\ 1 & 0 & 0 & 0 \end{pmatrix}.
 \end{aligned} \tag{6}$$

For the algebra of SU(4) and Sp(4) we have respectively

- $su(4) = \text{Span}\{T^1, T^2, \dots, T^{15}\}$,
- $sp(4) = \text{Span}\{T^6, T^7, \dots, T^{15}\}$.

The properties

$$\begin{aligned}
 \Omega T^A + T^{AT} \Omega &= 0 & A &= 6, \dots, 15, \\
 \Omega T^A - T^{AT} \Omega &= 0 & A &= 1, \dots, 5
 \end{aligned}$$

easily follow from Eq. (2).

The elementary theory we have investigated contains two flavours of Dirac fermions Q_a^i (with the index i identifying the flavour and a the colour Sp(4) component) transforming under the fundamental representation of Sp(4) and the gauge fields V_μ . Due to the fact that Sp(4) is pseudoreal, the global symmetry is enhanced from $SU(2)_L \times SU(2)_R$ to SU(4). With the above conventions on the generators understood and the transformation laws of the fields under Sp(4) gauge and global SU(4) given in Tab. 1, the Lagrangian density of the elementary theory is given by

$$\mathcal{L} = i \bar{Q}_a^i \gamma^\mu (D_\mu Q^i)^a - m \bar{Q}_a^i Q^{ia} - \frac{1}{2} \text{Tr} V_{\mu\nu} V^{\mu\nu}. \tag{7}$$

$V_{\mu\nu}$ is the field strength of the Sp(4) gauge bosons.

We can trade the two Dirac spinors for four left-handed Weyl components q^{ia} (see e.g. [17]). We then define the antisymmetric colour combination of two quarks (*diquark*)

$$\Sigma_0^{nm} \equiv \Omega_{ab} q^{naT} \tilde{C} q^{mb}, \tag{8}$$

where the colour indices a and b are contracted, while the flavour indices n and m (both running from one to four) are free.

When using the diquark fields as variables, the mass term is conveniently rewritten as $M \equiv m\Omega$. Hence, if a condensate forms, $\Sigma_0 \propto M$, which implies the global symmetry breaking pattern $SU(4) \mapsto Sp(4)$.

3 The effective field theory

The Chiral Lagrangian corresponding to our global symmetry breaking pattern can be written down using standard techniques. First, we define the field Σ transforming under the antisymmetric representation of $SU(4)$, i.e.

$$\Sigma \rightarrow U\Sigma U^T, \quad (9)$$

with U an element of global $SU(4)$. If Σ acquires a non-null vacuum expectation value ($v\epsilon v$), we will have (modulo an $SU(4)$ rotation)

$$\langle \Sigma \rangle \propto \Omega, \quad (10)$$

i.e. this vev will be responsible for the breaking $SU(4) \mapsto Sp(4)$. We can now introduce the parametrisation

$$\Sigma = e^{\frac{i\pi}{f}} \Omega e^{\frac{i\pi^T}{f}} = e^{\frac{2i\pi}{f}} \Omega = \Omega e^{\frac{2i\pi^T}{f}}. \quad (11)$$

In the chiral EFT approach, at the lowest order we can write

$$\begin{aligned} \mathcal{L}_0 &= \frac{f^2}{4} \text{Tr} \left\{ \partial_\mu \Sigma (\partial^\mu \Sigma)^\dagger \right\} \\ &= \text{Tr} \left\{ \partial_\mu \pi \partial^\mu \pi \right\} + \frac{1}{3f^2} \text{Tr} \left\{ [\partial_\mu \pi, \pi] [\partial^\mu \pi, \pi] \right\} + \dots, \end{aligned} \quad (12)$$

from which we immediately get the identification $f = f_\pi$.

In order to introduce a mass term, we define the spurion field M transforming as $M \rightarrow U^* M U^\dagger$, in terms of which we get the massive part of the Lagrangian

$$\mathcal{L}_m = -\frac{v^3}{4} \text{Tr} \{ M \Sigma \} + \text{h.c.} = 2mv^3 - \frac{mv^3}{f^2} \text{Tr} \pi^2 + \frac{mv^3}{3f^4} \text{Tr} (\pi\pi\pi\pi) + \dots. \quad (13)$$

From this equation we deduce that the pions are degenerate and that the GMOR relation

$$m_\pi^2 f_\pi^2 = m v^3 \quad (14)$$

holds.

The framework of hidden local symmetry [18] provides a prescription to include in the effective Lagrangian the vector (ρ) and the axial-vector (a_1) mesons. The procedure (represented by the moose diagram of Fig. 1) consists in the following steps:

1. We redefine the $SU(4)$ group under which Σ transforms in the antisymmetric representation as $SU(4)_A$:

$$\Sigma \rightarrow U_A \Sigma U_A^T; \quad (15)$$

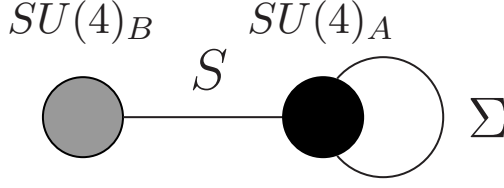


Figure 1. The moose diagram representing the hidden local symmetry construction for our model.

2. We introduce the scalar mesons σ by defining $S = e^{\frac{2i\sigma}{F}}$ and couple S bilinearly to the (conjugated) $SU(4)_A$ on the right and to an additional global $SU(4)_B$ on the left:

$$S \rightarrow U_B S U_A^\dagger; \quad (16)$$

3. We gauge $SU(4)_A$ and a $SU(2)_L \times U(1)_Y \subset \text{Sp}(4) \subset SU(4)_B$.

The covariant derivatives of the gauge theory take the forms

$$D_\mu S = \partial_\mu S + i(gW_\mu + g'B_\mu)S - iSg_\rho A_\mu; \quad (17)$$

$$D_\mu \Sigma = \partial_\mu \Sigma + i \left[(g_\rho A_\mu) \Sigma + \Sigma (g_\rho A_\mu)^T \right]. \quad (18)$$

It is now straightforward to determine the field content of the theory, consisting of 19 gauge bosons (15 A_μ , three W_μ and one B_μ) and 20 pseudoscalar fields (five π and 15 σ)

Following a standard procedure that we will detail elsewhere, we arrive at the following effective Lagrangian:

$$\begin{aligned} \mathcal{L} = & -\frac{1}{2} \text{Tr} B_{\mu\nu} B^{\mu\nu} - \frac{1}{2} \text{Tr} W_{\mu\nu} W^{\mu\nu} - \frac{1}{2} \text{Tr} A_{\mu\nu} A^{\mu\nu} - \frac{\kappa}{2} \text{Tr} \left[A_{\mu\nu} \Sigma (A^{\mu\nu})^T \Sigma^* \right] \\ & + \frac{f^2}{4} \text{Tr} \left[D_\mu \Sigma (D^\mu \Sigma)^\dagger \right] + \frac{F^2}{4} \text{Tr} \left[D_\mu S (D^\mu S)^\dagger \right] \\ & + b \frac{f^2}{4} \text{Tr} \left\{ D_\mu (S \Sigma) (D^\mu (S \Sigma))^\dagger \right\} + c \frac{f^2}{4} \text{Tr} \left\{ D_\mu (S \Sigma S^T) (D^\mu (S \Sigma S^T))^\dagger \right\} \\ & - \frac{v^3}{8} \text{Tr} \left\{ M S \Sigma S^T \right\} + \text{h.c.} \\ & - \frac{v_1}{4} \text{Tr} \left\{ M (D_\mu S) \Sigma (D^\mu S)^T \right\} - \frac{v_2}{4} \text{Tr} \left\{ M S (D_\mu \Sigma) (D^\mu S)^T \right\} + \text{h.c.} \\ & - \frac{y_3}{8} \text{Tr} \left\{ A_{\mu\nu} \Sigma \left[(A^{\mu\nu})^T S^T M S - S^T M S A^{\mu\nu} \right] \right\} + \text{h.c.} \\ & - \frac{y_4}{8} \text{Tr} \left\{ A_{\mu\nu} \Sigma \left[(A^{\mu\nu})^T S^T M S + S^T M S A^{\mu\nu} \right] \right\} + \text{h.c.} \\ & - \frac{v_5^2}{128} \left(\text{Tr} M S \Sigma S^T + \text{h.c.} \right)^2. \end{aligned} \quad (19)$$

In the low momentum expansion, the order is determined by pairs of derivatives, which are equivalent to mass insertions. Using this counting rule, we identify the leading terms in the first four lines of the previous equation. The corresponding couplings are the parameters κ, f, F, b, c, v . The last four lines contain some of the subleading terms. Computing all the subleading terms is a demanding

calculation. Hence, we have determined only those that we expect should be relevant for the study of mesonic two-point functions.

It is important to stress that the effective theory introduced above is only valid if $g_\rho^2/(4\pi)^2 \ll 1$. This can be checked *a posteriori*, by fitting the couplings and the other parameters of the low-energy theory through a match with observables derived from the fundamental theory. The ability of the derived low-energy theory to describe observables of the elementary theory at large distances is also a test of validity of the performed truncation. Writing down the relevant observables in the EFT and performing the relevant calculations (e.g. determining the positions of the poles of the two-point functions in momentum space in order to identify meson masses), we arrive to relations between parameters of the effective Lagrangian and physical observables. These include the following:

$$\begin{aligned}
M_\rho^2 &= \frac{1}{4(1 + \kappa + m y_3)} g_\rho^2 (b f^2 + F^2 + 2m v_1) , \\
M_{a_1}^2 &= \frac{1}{4(1 - \kappa - m y_4)} g_\rho^2 (b f^2 + F^2 + 2m v_1) + \frac{g_\rho^2}{1 - \kappa} (f^2 + m(v_2 - v_1)) , \\
f_\rho^2 &= \frac{1}{2} (b f^2 + F^2 + 2m v_1) , \\
f_{a_1}^2 &= \frac{(b f^2 - F^2 + 2m(v_1 - v_2))^2}{2((b + 4)f^2 + F^2 - 2m v_1 + 4m v_2)} , \\
f_0^2 &= F^2 + (b + 2c)f^2 , \\
f_\pi^2 &= f_0^2 - f_\rho^2 - f_{a_1}^2 .
\end{aligned} \tag{20}$$

Other calculable quantities that for brevity we do not write explicitly here include m_π , $g_{\rho\pi\pi}$, which is related to g_ρ , the Weinberg sum rules and the S parameter. Explicit expressions for those quantities will be reported in a forthcoming publication.

In the next two sections we describe lattice calculations that will be used to match the EFT with the elementary theory.

4 Lattice action and observables

The lattice action considered in this work is the standard plaquette action along with the unimproved Wilson Dirac fermions in the fundamental representation,

$$S[U] = \beta \sum_{\mu < \nu} \left(1 - \frac{1}{4} \text{Re Tr } U_\mu(x) U_\nu(x + \hat{\mu}) U_\mu^\dagger(x + \hat{\nu}) U_\nu^\dagger(x) \right) + a^4 \sum_x \bar{\psi}(x) (D + m_0) \psi(x), \tag{21}$$

where $\beta = 8/g^2$ and m_0 are the bare lattice gauge coupling and the bare fermion mass, respectively. Note that the link variables $U_\mu(x)$ are elements of the $\text{Sp}(4)$ group. The massless Wilson-Dirac operator is given by

$$aD\psi(x) = 4\psi(x) - \frac{1}{2} \sum_\mu \{ (1 - \gamma_\mu) U_\mu(x) \psi(x + \hat{\mu}) + (1 + \gamma_\mu) U(x - \hat{\mu}) \psi(x - \hat{\mu}) \}, \tag{22}$$

where a is the lattice spacing. The implementations of the heat bath (HB) algorithm for the pure gauge model and of the hybrid Monte-Carlo (HMC) algorithm in the dynamical fermion case of the lattice system described by the action in Eq. (21) are discussed respectively in [15] and in [16]. An essential technical difference from the case in which the gauge group is $\text{SU}(N)$ is a consequence of the fact

that $\text{Sp}(4)$ configurations span the maximal symplectic subgroup space of $\text{SU}(4)$, which means that reunitarisation must be replaced by resymplectisation.

To take full advantage of the EFT results derived in Sect. 3, we measure the masses and decay constants of pseudoscalar, vector, and axial-vector mesons. As such mesons can be defined in the isotriplet channel, it is sufficient to consider flavoured particles with the corresponding interpolating operators given by

$$\mathcal{O}_{\text{PS}}(x) = \bar{Q}^i(x)\gamma_5 Q^j(x), \quad \mathcal{O}_{\text{V}}(x) = \bar{Q}^i(x)\gamma_\mu Q^j(x), \quad \mathcal{O}_{\text{AV}}(x) = \bar{Q}^i\gamma_5\gamma_\mu Q^j, \quad (23)$$

where $i \neq j$ are flavour indices. Although not explicitly shown, summations over the colour and spinor indices are understood.

For the given mesonic operator \mathcal{O}_M the Euclidean two-point correlation function on a $T \times L^3$ lattice is defined as

$$C_{\mathcal{O}_M}(\vec{p}, t) = \sum_{\vec{x}} e^{-i\vec{p}\cdot\vec{x}} \langle 0 | \mathcal{O}_M(\vec{x}, t) \mathcal{O}_M^\dagger(\vec{0}, 0) | 0 \rangle, \quad (24)$$

where the meson mass m_M is extracted from the asymptotic behaviour of the correlator at large Euclidean time and zero momentum

$$C_{\mathcal{O}_M}(t) \xrightarrow{t \rightarrow \infty} \langle 0 | \mathcal{O}_M | M \rangle \langle 0 | \mathcal{O}_M | M \rangle^* \frac{1}{m_M L^3} \left[e^{-m_M t} + e^{-m_M(T-t)} \right]. \quad (25)$$

To calculate the decay constants f_M we parameterise the matrix elements of mesons as follows:

$$\langle 0 | \bar{Q}_1 \gamma_5 \gamma_\mu Q_2 | PS \rangle = i f_\pi p_\mu, \quad \langle 0 | \bar{Q}_1 \gamma_\mu Q_2 | V \rangle = i f_\rho m_\rho \epsilon_\mu, \quad \langle 0 | \bar{Q}_1 \gamma_5 \gamma_\mu Q_2 | AV \rangle = i f_{a_1} m_{a_1} \epsilon_\mu, \quad (26)$$

where ϵ_μ is the polarisation vector transverse to the four-momentum, i.e. $\epsilon_\mu p^\mu = 0$. The meson states $|M\rangle$ are the self-adjoint isospin fields, not the charged meson fields, as the corresponding pion decay constant in QCD is $f_\pi \simeq 93 \text{ MeV}$ in our convention. For the vector and axial-vector mesons, it is straightforward to calculate the masses and decay constants from the asymptotic forms of $C_{\mathcal{O}_M}(t)$ in Eq. (25) using the parameterisations in Eq. (26). In the case of the pseudoscalar meson, along with the pseudoscalar two-point correlation function, we consider an additional correlation function

$$C_\Pi(\vec{p}, t) = \sum_{\vec{x}} e^{-i\vec{p}\cdot\vec{x}} \langle 0 | [\bar{Q}_1 \gamma_5 \gamma_\mu Q_2(\vec{x}, t)] [\bar{Q}_1 \gamma_5 Q_2(\vec{0}, 0)] | 0 \rangle. \quad (27)$$

Using the fact that this correlation function is dominated by the lowest mass pseudoscalar state at large time, one can find

$$C_\Pi(\vec{p}, t) \xrightarrow{t \rightarrow \infty} \frac{i f_\pi \langle 0 | \mathcal{O}_{PS} | PS \rangle^*}{L^3} \left[e^{-m_\pi t} - e^{-m_\pi(T-t)} \right], \quad (28)$$

where m_π and f_π are determined from the simultaneous fits for $C_\Pi(\vec{p}, t)$ and $C_{\text{PS}}(\vec{p}, t)$.

To convert the measured quantities in lattice units to physical ones in the continuum, an appropriate scale setting and renormalisation are required. For the latter, in this work, we renormalise the decay constants by performing a perturbative one-loop matching. For Wilson fermions the decay constants receive finite multiplicative renormalisation as

$$f_\pi^{\text{ren}} = Z_A f_\pi, \quad f_\rho^{\text{ren}} = Z_V f_\rho, \quad \text{and} \quad f_{a_1}^{\text{ren}} = Z_A f_{a_1}, \quad (29)$$

where the matching coefficients are calculated in Ref. [19]

$$\begin{aligned} Z_A &= 1 + C(F) (\Delta_{\Sigma_1} + \Delta_{\gamma_5 \gamma_\mu}) \frac{\tilde{g}^2}{16\pi^2}, \\ Z_V &= 1 + C(F) (\Delta_{\Sigma_1} + \Delta_{\gamma_\mu}) \frac{\tilde{g}^2}{16\pi^2}, \end{aligned} \quad (30)$$

	w_0	plaquette	Z_V	Z_A
$b = 7.62$	1.448(4)	0.60190(19)	0.71599(9)	0.78157(7)
$b = 8.0$	2.308(6)	0.63074(13)	0.74185(5)	0.80146(4)

Table 2. Gradient flow scales w_0 , plaquette values and one-loop matching factors Z_V and Z_A at the values of β used in our quenched calculation.

with $C(F) = 5/4$ for the $\text{Sp}(4)$ theory with fundamental fermions. The Δ 's are results of relevant one-loop integrals performed numerically. Their values are

$$\Delta_{\Sigma_1} = -12.82, \quad \Delta_{\gamma_\mu} = -7.75, \quad \Delta_{\gamma_5\gamma_\mu} = -3.00. \quad (31)$$

Furthermore, as the perturbative expansion for Wilson fermions with a bare lattice coupling converges slowly, we use the coupling renormalised by a simple Tadpole improvement

$$\tilde{g} = \frac{g^2}{\langle \text{tr}\mathcal{P} \rangle / 4}, \quad (32)$$

where \mathcal{P} is the usual plaquette operator.

For the scale setting we adapt the gradient flow method with the choice of $\mathcal{W}(\bar{t}) \equiv t \, d\mathcal{E}(\bar{t})/dt$, where as the scale-setting observable a symmetric four-plaquette clover has been used for the discretisation of the action density $\mathcal{E}(\bar{t})$ at the fictitious flow time \bar{t} . A comparison of this with other potential choices is discussed in [16].

5 Numerical results in the quenched limit

Although the effects of fermions are not properly captured in the quenched approximation, the latter is often studied to understand the qualitative features of the full theory, an obvious advantage being the possibility of performing calculations using comparatively smaller computational resources. For instance, in the quenched framework one can test the low-energy EFT in Sect. 2 and demonstrate its use by calculating the associated mesonic observables. To this end, using the HB algorithm implemented to the HiRep code [20, 21], we generate two ensembles of pure $\text{Sp}(4)$ gauge theory at $\beta = 7.62$ and 8.0 on a 48×24^3 lattice with 200 independent configurations in each case. To convert the measured lattice quantities to the physical ones, we first calculate the gradient flow scale w_0 and the one-loop matching constants, for which the numerical results are found in Tab. 2. Note that our choice for the reference scale in the scale-setting procedure is $\mathcal{W}(\bar{t})|_{\bar{t}=w_0^2} = \mathcal{W}_0 = 0.35$.

At various fermion masses we calculate the two-point correlation functions of mesons in Eq. (24) at zero momentum using stochastic wall sources. If the Euclidean time is large enough, in principle, one can extract the masses and the decay constants using the asymptotic forms of the correlation functions in Eqs. (25) and (28). If the time separation is not long enough, however, one should take into account the contribution of excited states, which translates into considering a multi-exponential behaviour. In most cases we find that single and two exponential fits are sufficient to describe the numerical data at large time. A correlated fit with χ^2 minimisation is used to calculate the masses and decay constants, where the statistical uncertainties are estimated using the standard bootstrapping technique. We show our numerical results in Tabs. 3 and 4. In order to apply an analysis based on the continuum EFT to the numerical results, we should express observables in physical units by

Table 3. Masses and bare decay constants of pseudoscalar, vector and axial-vector mesons for quenched calculations performed at $\beta = 7.62$ on a 48×24^3 lattice.

m_0	m_{PS}^2	m_{V}^2	m_{AV}^2	f_{PS}^2	f_{V}^2	f_{AV}^2
-0.65	0.4325(5)	0.5087(8)	1.04(4)	0.01451(9)	0.0376(3)	0.021(4)
-0.7	0.3042(4)	0.3916(11)	0.943(29)	0.01246(8)	0.0365(4)	0.029(3)
-0.73	0.2318(4)	0.3272(14)	0.862(20)	0.01101(8)	0.0354(5)	0.0313(20)
-0.75	0.1856(4)	0.2875(15)	0.831(16)	0.00995(8)	0.0346(4)	0.0352(16)
-0.77	0.1409(4)	0.2485(19)	0.769(22)	0.00879(8)	0.0329(6)	0.0350(22)
-0.78	0.1191(4)	0.2312(21)	0.796(17)	0.00822(8)	0.0327(6)	0.0415(16)
-0.79	0.0977(4)	0.2115(26)	0.772(20)	0.00760(8)	0.0314(8)	0.0418(19)
-0.8	0.0765(4)	0.193(3)	0.748(24)	0.00698(8)	0.0301(10)	0.0417(23)
-0.81	0.0553(4)	0.175(5)	0.73(3)	0.00635(9)	0.0285(14)	0.042(3)
-0.815	0.0446(4)	0.166(7)	0.70(4)	0.00606(9)	0.0280(19)	0.040(4)
-0.82	0.0328(4)	0.158(13)	0.70(6)	0.00572(15)	0.028(4)	0.041(6)

Table 4. Masses and bare decay constants of pseudoscalar, vector, and axial-vector mesons for quenched calculations performed at $\beta = 8.0$ on a 48×24^3 lattice.

m_0	m_{PS}^2	m_{V}^2	m_{AV}^2	f_{PS}^2	f_{V}^2	f_{AV}^2
-0.45	0.5556(12)	0.5837(13)	0.868(13)	0.00832(14)	0.01528(27)	0.0057(5)
-0.5	0.4244(11)	0.4551(14)	0.734(11)	0.00771(14)	0.0149(3)	0.0073(6)
-0.55	0.3037(8)	0.3383(12)	0.593(11)	0.00691(10)	0.0145(3)	0.0084(7)
-0.6	0.1937(8)	0.2325(14)	0.465(12)	0.00567(8)	0.0131(3)	0.0096(8)
-0.625	0.1437(7)	0.1862(16)	0.405(13)	0.00494(8)	0.0125(4)	0.0102(10)
-0.64	0.1156(7)	0.1612(15)	0.363(20)	0.00449(7)	0.0124(3)	0.0099(18)
-0.65	0.0974(7)	0.1448(16)	0.349(15)	0.00414(7)	0.0120(3)	0.0109(13)
-0.66	0.0812(5)	0.1302(14)	0.343(14)	0.00397(5)	0.0123(3)	0.0128(12)
-0.67	0.0642(5)	0.1179(18)	0.318(18)	0.00352(4)	0.0123(4)	0.0123(17)
-0.68	0.0479(4)	0.1040(22)	0.323(13)	0.00319(4)	0.0122(5)	0.0150(11)
-0.69	0.0318(4)	0.0907(28)	0.304(19)	0.00270(5)	0.0115(5)	0.0151(17)

multiplying by the (length) scale w_0 the quantities having mass dimension one and take into account the multiplicative renormalisation for the decay constants.

By restricting our attention to the pseudoscalar mesons and using the GMOR relation we first determine the critical fermion mass at which m_{PS} vanishes. As the numerical results of $m_{\text{PS}}^2, f_{\text{PS}}^2$ do not show the validity of the leading order GMOR relation, we perform quadratic fits over the bare mass range $-0.82 \leq m_0 \leq -0.73$ for $\beta = 7.62$ and $-0.69 \leq m_0 \leq -0.625$ for $\beta = 8.0$, and find $-w_0 m_0^* = -1.214(22)$ and $-w_0 m_0^* = -1.636(27)$, respectively. The resulting GMOR relation is illustrated in the left panel of Fig. 2. Note that the results with different lattice coupling (or equivalently different lattice spacing) cannot be compared directly, as the quark mass renormalisation depends on β . One can overcome this problem by simply considering a physical (and hence free from renormalisation) quantity such as the pseudoscalar mass m_{PS} . In the right panel of Fig. 2 we replot $m_{\text{PS}}^2, f_{\text{PS}}^2$ with respect to m_{PS} , and find that the GMOR relations at the two lattice couplings are statistically identical. In other words, the lattice artefacts due to finite lattice spacing are negligible in the GMOR relation.

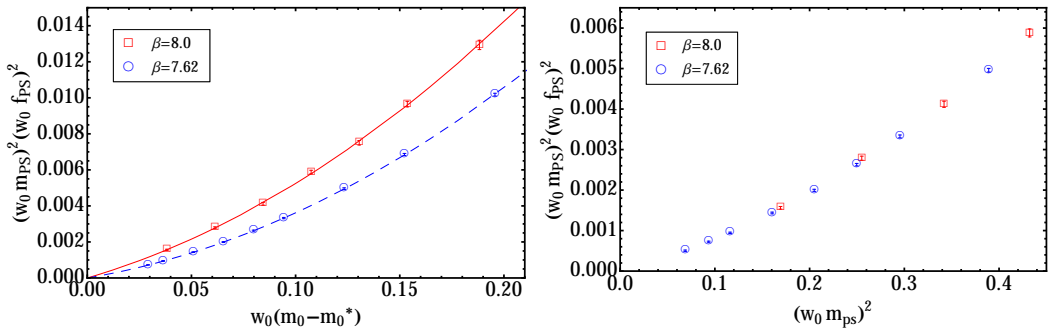


Figure 2. Product of mass squared and decay constant squared for the pseudoscalar meson. Scale setting with the gradient flow method and perturbative one-loop matching for the decay constants are understood. In the left panel, $m_{\text{PS}}^2 f_{\text{PS}}^2$ is measured with respect to the bare fermion mass shifted by the critical mass, m_0^* , with the latter determined from quadratic fits. The solid and dashed lines are the fit results. In the right panel, the same combination is measured with respect to the squared pseudoscalar mass. All quantities are expressed in units of w_0 .

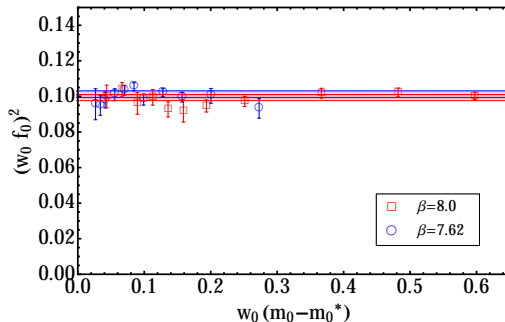


Figure 3. Sum of the squared decay constants of the pseudoscalar, vector and axial-vector mesons. The coloured band denotes the (constant) fit result with statistical error for each lattice gauge coupling.

Among the physical observables in the (tree-level) NLO EFT, the sum of the squared decay constants of pseudoscalar, vector and axial-vector mesons parameterised by f_0^2 is expected to be mass-independent. In principle, the tree-level result can be corrected by the chiral one-loop effects including chiral logarithms. This would result in a non-trivial mass dependence of f_0^2 . However, this does not happen: as the NLO mass term plays the role of the counter term that cancels the UV divergence in the chiral logarithms, no additional mass dependence appears as long as the tree level result is independent on the fermion mass. Indeed, as seen in Fig. 3, we numerically confirmed this EFT result for f_0^2 . Note that the mass independence of f_0^2 seems to be a feature that persists even for heavy fermions. We therefore perform a constant fit to the data, and find $f_0^2 = 0.1012(19)$ and $f_0^2 = 0.0993(17)$ for $\beta = 7.62$ and 8.0 , respectively. This result further suggests that the lattice artefacts in f_0^2 are negligible.

The primary purpose of our numerical programme here is to determine the low-energy constants appearing in the low-energy NLO EFT developed in Sect. 3, and we use the quenched data to test

the applicability of this approach to generic Sp(4) theories with dynamical fermions. We therefore perform a (uncorrelated) global fit to the data for the masses and decay constants of pseudoscalar, vector and axial-vector mesons using the formulae in Eq. (20). The fitting ranges are restricted to the eight and six lightest fermion masses for $\beta = 7.62$ and 8.0, respectively, as we do not expect the NLO EFT to describe correctly the heavy fermion regime. Using the standard fit procedure employing a χ^2 minimisation, we are confronted with two technical obstacles. First of all, statistical uncertainties for different types of mesons vary widely; hence, the fit results are essentially constrained by the pseudoscalar mesons. Secondly, the global fits are not stable, because the parameter space of the NLO EFT, which contains thirteen parameters including the critical fermion mass, is too large for us to be able to determine the actual global minimum.

Despite these caveats, as the purpose of the quenched calculation is to illustrate the usage of our EFT, we attempt to perform the global fit to the central values. Because of uncontrolled systematics such as discretisation and quenching effects, we do not expect to extract the physical information from this explorative study. The results are illustrated in Fig. 4 taking the coarse lattice ($\beta = 7.62$) as an example. The extracted fit values are

$$\begin{aligned} \kappa = -0.76, y_3 = -0.61, y_4 = 3.21, g_c = 2.14, b = -0.42, c = -0.031, f_1 = 0.74, f_2 = 0.55, \\ v_1 = 0.088, v_2 = -0.31, v = 0.27, v_5 = 0.40, m_0^* = -1.21, \chi^2/\text{d.o.f} = 0.74, \end{aligned} \quad (33)$$

for $\beta = 7.62$ and

$$\begin{aligned} \kappa = -0.87, y_3 = -0.35, y_4 = 2.75, g_c = 1.74, b = -0.30, c = -0.012, f_1 = 0.97, f_2 = 0.60, \\ v_1 = 0.034, v_2 = -0.30, v = 0.28, v_5 = 0.48, m_0^* = -1.64, \chi^2/\text{d.o.f} = 0.97, \end{aligned} \quad (34)$$

for $\beta = 8.0$, respectively, where all of these fit results satisfy the unitarity conditions.

The NLO EFT also allows us to compute the Peskin-Takeuchi S -parameter and the ρ - π - π coupling in the massless limit,

$$\begin{aligned} S/4\pi \sim 0.065, \quad g_{\rho\pi\pi}^2/(48\pi) \sim 0.9 \quad \text{for } \beta = 7.62, \\ S/4\pi \sim 0.053, \quad g_{\rho\pi\pi}^2/(48\pi) \sim 1.2 \quad \text{for } \beta = 8.0. \end{aligned} \quad (35)$$

The resulting S parameters of Sp(4) theories are larger than the QCD values of $S/4\pi \sim 0.025$ computed in the same way (i.e. the zeroth sum rule, $S/4\pi = f_V^2/M_V^2 - f_{AV}^2/M_{AV}^2$). This result agrees with our naive expectation based on the fact that the dimension of the gauge group is larger than that of QCD. In addition, the S parameter seems to decrease as $a \rightarrow 0$. It is worth stressing once again that one cannot take these results too literally because the lattice artefacts and quenching effects are not fully accounted for. Similarly, the large values of $g_{\rho\pi\pi}$ are presumably due to the quenching effects.

As we learned from the meson spectrum in the pseudoscalar sector, it is useful to calculate mesonic quantities as a function of the pseudoscalar mass to avoid the cumbersome renormalization procedure for the fermion mass. As shown in Fig. 5, the lattice spacing artefacts are quite large for the vector mesons, while those are negligible for the pseudoscalar and axial-vector mesons.

6 Toward dynamical simulations

To the best of our knowledge, the Sp(4) theory with dynamical $N_f = 2$ Wilson fermions has not been studied before in the literature. Therefore, first and foremost, we need to investigate the phase structure in the lattice parameter space in order to look for potential first order bulk transitions. From such studies one can identify the (weak coupling) phase that is analytically connected to the continuum theory as $a \rightarrow 0$. Since one cannot consider an arbitrarily small a and an arbitrarily large lattice

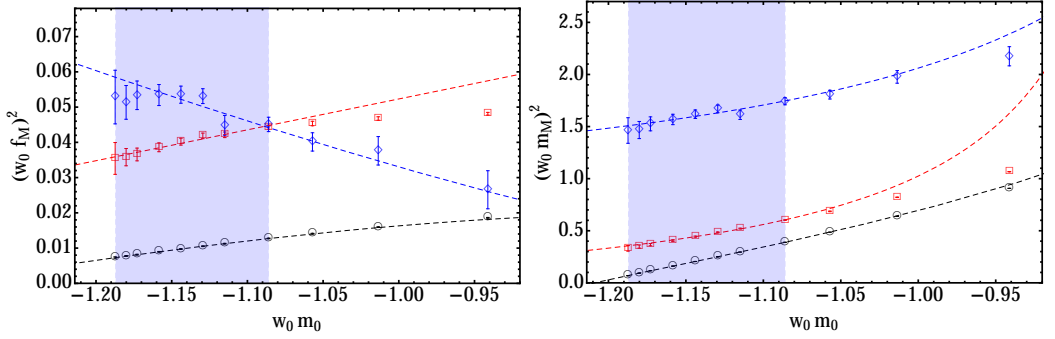


Figure 4. Masses and decay constants of pseudoscalar (black empty circle), vector (red empty square) and axial-vector (blue empty diamond) mesons in the quenched $Sp(4)$ at $\beta = 7.62$, measured with respect to the fermion mass. Scale setting with the gradient flow method and perturbative one-loop matching for the decay constants are understood. A global fit has been performed simultaneously using all the measured masses and decay constants over the range of the bare fermion mass $-0.82 \leq m_0 \leq -0.75$, with $w_0 = 1.448$. The dashed lines denote the fit results.

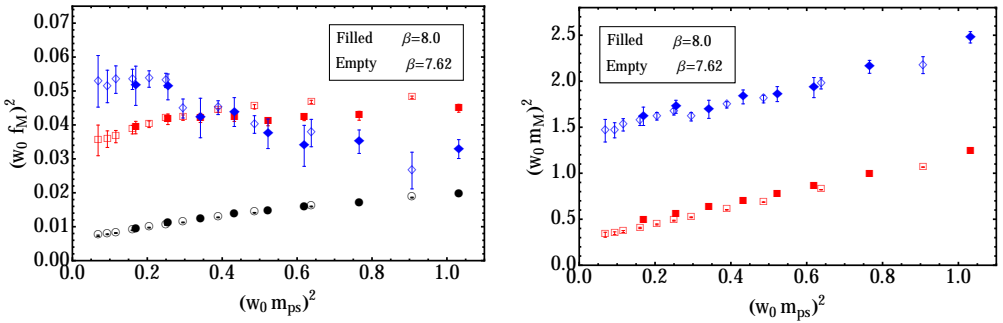


Figure 5. Masses and decay constants of pseudoscalar (black circle), vector (red square) and axial-vector (blue diamond) mesons in the quenched $Sp(4)$ at $\beta = 7.62$ (empty) and 8.0 (filled), measured with respect to the pseudoscalar mass squared. Scale setting with the gradient flow method and perturbative one-loop matching for the decay constants are understood.

volume V , the identification of the phase boundary is also an important task from the practical point of view.

The order parameter associated with the lattice bulk transition is the expectation value of the plaquette. In Fig. 6, we show the mass scan of the two-flavour $Sp(4)$ theory using a 4^4 lattice. For each lattice coupling β chosen between 6.0 and 7.0 we vary the fermion mass in steps of 0.1 over the range $0.0 \leq -am_0 \leq 1.4$. For the region, where the average plaquette values change rapidly as m_0 changes, we increase the resolution by a factor of two. At small values of $\beta \approx 6.6$ the plaquette values change abruptly, indicating the existence of a bulk phase. To accurately determine the phase boundary, we further study the finite size scaling of the plaquette susceptibility χ at $\beta = 6.6$ and 6.8

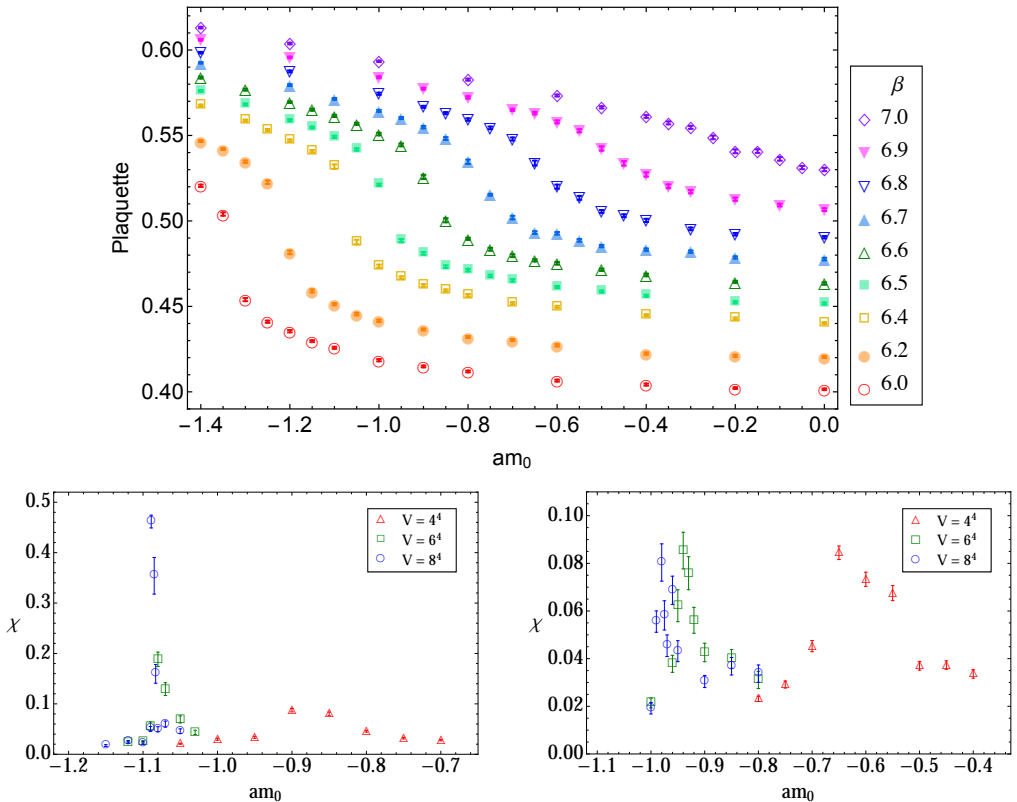


Figure 6. (top) Structure of a phase space in the Sp(4) theory with two flavour (mass degenerated) dynamical Wilson fermions on a 4^4 lattice. The x - and y -axes are the expectation values of the plaquette and the bare fermion mass. Different colours correspond to the lattice gauge couplings. (bottom) Plaquette susceptibilities versus bare fermion mass at $\beta = 6.6$ (left) and $\beta = 6.8$ (right). Three hypercubic lattices are considered, 4^4 (red triangle), 6^4 (green square) and 8^4 (blue square).

by considering a 4^4 , 6^4 , and 8^4 lattice. χ is defined as

$$\chi = \sum_x \langle \mathcal{P}(0) \mathcal{P}(x) \rangle = (\langle \mathcal{P}^2 \rangle - \langle \mathcal{P} \rangle^2) V. \quad (36)$$

As shown in Fig. 6, the maximum values of χ for $\beta = 6.6$ roughly scale with V indicating a first order bulk phase transition, while those for $\beta = 6.8$ roughly constant as a function of V , clearly indicating a crossover behaviour. We therefore conclude that we can safely take the continuum limit for $\beta \geq \beta^* \simeq 6.8$. Note that in the case of pure Sp(4) theory formulated with the standard plaquette action bulk phase transitions do not arise.

Based on our finding on the phase boundary, we use the coarse lattice with $\beta = 6.9$ to test the stability of dynamical simulations and provide a very preliminary understandings of the meson spectrum. We generate five ensembles using the HMC algorithm, $m_0 = -0.85, -0.87$ on a 24×12^3 and $m_0 = -0.89, -0.9, -0.92$ on a 32×16^3 lattices. As shown in the left panel of Fig. 7, the trajectories of the average plaquettes are stable and their asymptotic values increase as the fermion mass decreases.

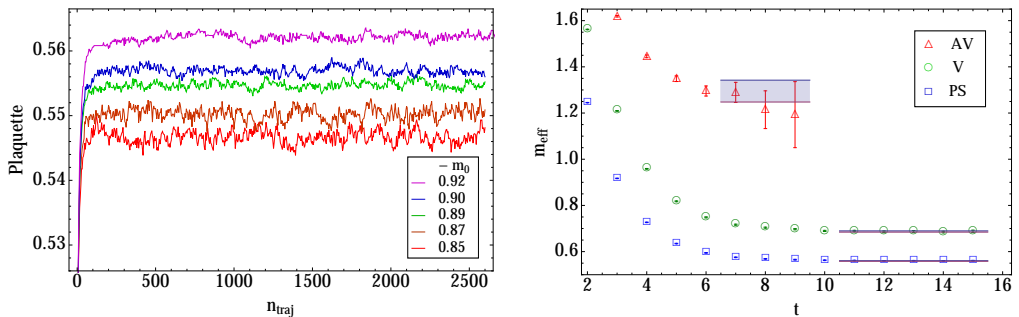


Figure 7. (left) Plaquette trajectories at various bare fermion masses and lattice coupling of $\beta = 6.9$. The lightest three fermion masses are simulated on a 32×16^3 , while the remaining masses are simulated on a 24×12^3 . (right) Plot of effective masses for pseudoscalar, vector and axial-vector mesons at $\beta = 6.9$ with $m_0 = -0.9$ on a 32×16^3 lattice.

While the thermalisation time typically appears to be ~ 300 , the autocorrelation time varies between 12 and 32, depending on the ensembles.

To illustrate how to extract meson masses from the two-point correlation functions, in the right panel of Fig. 7, we show the effective mass plots for pseudoscalar, vector and axial-vector mesons with $m_0 = -0.9$. By performing a constant fit to the plateau region at large time, we determine the meson masses. The masses of the pseudoscalar and vector mesons are smaller than the UV cutoff with $m_{PS}/m_V \sim 0.8$, while the mass of the axial-vector is at the UV scale. Although this explorative study in the dynamical fermion case does not provide much physical information, in the future it will certainly guide us towards more interesting numerical findings for the $N_f = 2$ Sp(4) theory, which will enable us to perform an EFT analysis similar to the one discussed in the previous section.

7 Conclusion

In this contribution, we have investigated the global symmetry breaking pattern $SU(4) \mapsto Sp(4)$ in the language of effective field theory and, using Sp(4) gauge theory coupled to two fundamental Dirac fermions, we have discussed the determination of the corresponding low-energy constants. Our investigation provides encouraging evidence that a similar line of study can be pursued also for the model with dynamical fermions, for which we have presented first results in this work. As a next step in our programme, we shall extend the lattice calculation in the dynamical system with the longer term goal of obtaining the low-energy constants of the effective field theory with a controlled systematics and enough statistical accuracy to make our results relevant for phenomenology.

Acknowledgements

We acknowledge the support of the Supercomputing Wales project, which is part-funded by the European Regional Development Fund (ERDF) via Welsh Government.

References

- [1] D.B. Kaplan, H. Georgi, S. Dimopoulos, Phys. Lett. **136B**, 187 (1984)

- [2] G. Panico, A. Wulzer, *Lect. Notes Phys.* **913**, pp.1 (2016), 1506.01961
- [3] M.E. Peskin, *Nucl. Phys.* **B175**, 197 (1980)
- [4] J. Barnard, T. Gherghetta, T.S. Ray, *JHEP* **02**, 002 (2014), 1311.6562
- [5] G. Ferretti, D. Karateev, *JHEP* **03**, 077 (2014), 1312.5330
- [6] G. Ferretti, *JHEP* **06**, 107 (2016), 1604.06467
- [7] L. Vecchi, *JHEP* **02**, 094 (2017), 1506.00623
- [8] B. Svetitsky, *Looking behind the Standard Model with lattice gauge theory*, in Proceedings, **35th International Symposium on Lattice Field Theory (Lattice2017)**: Granada, Spain, *to appear in EPJ Web Conf.* (2017), 1708.04840
- [9] T. DeGrand, Y. Liu, E.T. Neil, Y. Shamir, B. Svetitsky, *Phys. Rev.* **D91**, 114502 (2015), 1501.05665
- [10] R. Arthur, V. Drach, M. Hansen, A. Hietanen, C. Pica, F. Sannino, *Phys. Rev.* **D94**, 094507 (2016), 1602.06559
- [11] T.A. DeGrand, M. Golterman, W.I. Jay, E.T. Neil, Y. Shamir, B. Svetitsky, *Phys. Rev.* **D94**, 054501 (2016), 1606.02695
- [12] L. Del Debbio, C. Englert, R. Zwicky, *JHEP* **08**, 142 (2017), 1703.06064
- [13] V. Ayyar, T. DeGrand, D.C. Hackett, W.I. Jay, E.T. Neil, Y. Shamir, B. Svetitsky, *Chiral Transition of SU(4) Gauge Theory with Fermions in Multiple Representations*, in Proceedings, **35th International Symposium on Lattice Field Theory (Lattice2017)**: Granada, Spain, *to appear in EPJ Web Conf.* (2017), 1709.06190
- [14] V. Ayyar, T. DeGrand, M. Golterman, D.C. Hackett, W.I. Jay, E.T. Neil, Y. Shamir, B. Svetitsky (2017), 1710.00806
- [15] E. Bennett, D.K. Hong, J.W. Lee, C.J.D. Lin, B. Lucini, M. Piai, D. Vadacchino, *Higgs compositeness in Sp(2N) gauge theories — The pure gauge model*, in Proceedings, **35th International Symposium on Lattice Field Theory (Lattice2017)**: Granada, Spain, *to appear in EPJ Web Conf.* (2017)
- [16] E. Bennett, D.K. Hong, J.W. Lee, C.J.D. Lin, B. Lucini, M. Piai, D. Vadacchino, *Higgs compositeness in Sp(2N) gauge theories — Resymplecticisation, scale setting and topology*, in Proceedings, **35th International Symposium on Lattice Field Theory (Lattice2017)**: Granada, Spain, *to appear in EPJ Web Conf.* (2017)
- [17] J.W. Lee, B. Lucini, M. Piai, *JHEP* **04**, 036 (2017), 1701.03228
- [18] M. Bando, T. Kugo, S. Uehara, K. Yamawaki, T. Yanagida, *Phys. Rev. Lett.* **54**, 1215 (1985)
- [19] G. Martinelli, Y.C. Zhang, *Phys. Lett.* **123B**, 433 (1983)
- [20] L. Del Debbio, A. Patella, C. Pica, *Phys. Rev.* **D81**, 094503 (2010), 0805.2058
- [21] L. Del Debbio, B. Lucini, A. Patella, C. Pica, A. Rago, *Phys. Rev.* **D80**, 074507 (2009), 0907.3896